

Noradrenaline released from locus coeruleus axons contracts cerebral capillary pericytes via α_2 adrenergic receptors

Journal of Cerebral Blood Flow & Metabolism

0(0) 1–11

© The Author(s) 2023





Article reuse guidelines:

sagepub.com/journals-permissions

DOI: 10.1177/0271678X231152549

journals.sagepub.com/home/jcbfm

Nils Korte¹, Greg James^{1,2}, Haoming You¹,
Chanawee Hirunpattarasilp^{1,3}, Isabel Christie¹ , Huma Sethi⁴
and David Attwell¹ 

Abstract

Noradrenaline (NA) release from locus coeruleus axons generates vascular contractile tone in arteriolar smooth muscle and contractile capillary pericytes. This tone allows neuronal activity to evoke vasodilation that increases local cerebral blood flow (CBF). Much of the vascular resistance within the brain is located in capillaries and locus coeruleus axons have NA release sites closer to pericytes than to arterioles. In acute brain slices, NA contracted pericytes but did not raise the pericyte cytoplasmic Ca^{2+} concentration, while the α_1 agonist phenylephrine did not evoke contraction. Blocking α_2 adrenergic receptors (α_2 Rs, which induce contraction by inhibiting cAMP production), greatly reduced the NA-evoked pericyte contraction, whereas stimulating α_2 Rs using xylazine (a sedative) or clonidine (an anti-hypertensive drug) evoked pericyte contraction. Noradrenaline-evoked pericyte contraction and capillary constriction are thus mediated via α_2 Rs. Consequently, α_2 Rs may not only modulate CBF in health and pathological conditions, but also contribute to CBF changes evoked by α_2 R ligands administered in research, veterinary and clinical settings.

Keywords

Noradrenaline, locus coeruleus, pericyte, calcium, cAMP

Received 22 July 2022; Revised 15 November 2022; Accepted 3 January 2023

Introduction

Active neurons require an increased energy supply to power their information processing. This is achieved by the neurons, and their associated astrocytes, releasing vasodilating agents that increase local cerebral blood flow (CBF).¹ Within the cerebral cortex, although smooth muscle cells (SMCs) around arterioles contribute to regulating CBF, the majority of the vascular resistance is located in the capillary bed.^{2,3} Contractile pericytes, found especially on the first 3 branch orders of capillaries from arterioles (defined as 0th order), can adjust the capillary diameter to alter CBF, in health and in pathology.^{4–6}

In order for CBF to be increased by neuronal activity, there must be an ongoing tone generated by contractile mural cells, which are then relaxed in order to increase vessel diameter. A significant contribution to this tone is generated by the release of noradrenaline

from perivascular axon terminals of neurons with somata in the locus coeruleus and nearby nuclei.^{7,8} Two-thirds of these terminals are closer to capillaries rather than arterioles.⁹ Locus coeruleus axons also

¹Dept of Neuroscience, Physiology & Pharmacology, University College London, London, UK

²Department of Neurosurgery, Great Ormond Street Hospital, London, UK

³Princess Srisavangavadhana College of Medicine, Chulabhorn Royal Academy, Bangkok, Thailand

⁴Dept of Neurosurgery, National Hospital for Neurology and Neurosurgery, London, UK

Nils Korte's current address is: F.M. Kirby Neurobiology Center, Boston Children's Hospital and Harvard Medical School, Boston, MA, USA.

Corresponding author:

David Attwell, Dept of Neuroscience, Physiology & Pharmacology, University College London, Gower St., London, WC1E 6BT, UK.
Email: d.attwell@ucl.ac.uk

target astrocytes,⁹ which have been suggested to be key intermediaries in the regulation of CBF by neuronal activity.⁴ Thus, locus coeruleus derived noradrenaline may affect CBF by acting either directly on pericytes or SMCs, or indirectly via astrocytes. In brain slices, which presumably lack locus coeruleus noradrenaline release, superfusing noradrenaline constricts capillaries near pericyte somata (where the pericytes' circumferential processes are mainly found⁶) by ~60% in rat cerebellar cortex¹⁰ and by ~40% in human cerebral cortex.⁶

Surprisingly, the mechanism by which noradrenaline contracts pericytes is unknown. An obvious possibility is that noradrenaline activates G_q-linked α_1 receptors on pericytes which raise $[Ca^{2+}]_i$ and thus activate contraction, as for arteriole smooth muscle.¹¹ Alternatively, noradrenaline could act indirectly via astrocytes or neurons. For example noradrenaline raises astrocyte $[Ca^{2+}]_i$ by activating α_1 receptors,¹² and these have been suggested to generate constriction of arteriolar SMCs by evoking the release of the arachidonic acid derivative 20-HETE (20-hydroxyeicosatetraenoic acid) from astrocytic endfeet enwrapping vessels.¹³

Here we use transgenic mice expressing NG2-dsRed in pericytes, and human tissue from neurosurgical operations, to investigate how noradrenaline evokes pericyte-mediated constriction of cerebral cortical capillaries. We confirmed that locus coeruleus axon noradrenaline release sites are located close to pericyte somata⁹ in both mice and humans. Surprisingly, however, we found that the constricting actions of noradrenaline were mediated, not by α_1 receptors which raise $[Ca^{2+}]_i$, but by α_2 receptors which lower the intracellular cyclic AMP concentration.

Materials and methods

Animals

All animal procedures were performed in accordance with EU and UK regulations (the UK Animals (Scientific Procedures) Act 1986 and later modifications), and are described in accordance with the ARRIVE guidelines. Sprague Dawley rats of either sex were group-housed or kept in litters in open-top cages until experimental use for capillary brightfield imaging at P21. Mice were housed in individually ventilated cages in pairs or groups. Adult mice (P42-P158) of either sex were used. NG2-dsRed mice expressing a dsRed fluorophore under the NG2 proteoglycan promoter allowed visualisation of cells expressing NG2 including pericytes, smooth muscle cells (SMCs) and oligodendrocyte precursor cells (OPCs).¹⁴ NG2-Cre^{ERT2}-GCaMP5G mice were obtained by crossing⁶ tamoxifen-inducible NG2-Cre^{ERT2} knock in mice¹⁵

with floxed GCaMP5G-IRES-tdTomato mice¹⁶ to allow co-expression of the genetically-encoded Ca^{2+} indicator (GCaMP5G) and tdTomato fluorophore (as a morphological marker) in NG2-expressing cells after oral gavage of tamoxifen. Tamoxifen dissolved in corn oil was given at 100 mg/kg body weight by oral gavage once per day for four consecutive days to adult >P21 mice. Experiments were performed from 2 weeks after tamoxifen administration. Animals were maintained in a 12 h light/dark cycle, at controlled temperatures (20–23°C) and fed normal chow and untreated tap water ad libitum. Treated Aspen chip and Sizzle-Nest bedding and one tunnel for environmental enrichment were present in each cage. Animals were sacrificed by cervical dislocation for all experiments using acute cortical slices or by cardiac perfusion under terminal anaesthesia for immunohistochemistry. Animal breeding, experimental procedure and methods of killing were conducted in accordance with the UK Home Office regulations (Guidance on the Operation of Animals, Scientific Procedures Act, 1986) and the approval of UCL's Animal Welfare and Ethical Review Body.

Human tissue

Live human cortical tissue, removed to access underlying tumours in patients, was obtained from neurosurgery at the National Hospital for Neurology and Neurosurgery, Queen Square. Tissue was from 3 male glioblastoma patients (17, 66 and 67 years old) who gave written informed consent. Ethical standards were according to the Helsinki Declaration (World Medical Association, 1975, as amended in 2013) and ethical approval was from the National Health Service (North West Research Ethics Committee, approval 15/NW/0568).

Cortical tissue preparation

Cortical slices (300 μ m-thick) were prepared from P21 SD rats or P42-P116 NG2-Cre^{ERT2}-GCaMP5G mice on a Leica VT1200S vibratome in ice-cold, oxygenated (95% O₂/5% CO₂) slicing solution. The slicing solution contained (in mM) 93 N-methyl-D-glucamine chloride, 2.5 KCl, 30 NaHCO₃, 10 MgCl₂, 1.2 NaH₂PO₄, 25 glucose, 0.5 CaCl₂, 20 HEPES, 5 Na-ascorbate, 3 Na pyruvate, 1 kynurenic acid. The slices were incubated at 37°C in the slicing solution (20 min), and then transferred into a modified solution at room temperature in which the NMDG-Cl, MgCl₂, CaCl₂ and Na ascorbate were replaced by (in mM) 92 NaCl, 1 MgCl₂, 2 CaCl₂ and 1 Na-ascorbate. Experiments were performed within 3–4 hrs of sacrificing rodents. Human tissue obtained at the hospital was transported to the laboratory in ice-cold slicing solution and incubated for

~2 hours in oxygenated HEPES-buffered solution containing 10 $\mu\text{g/ml}$ isolectin B4 (IB4) conjugated to Alexa FluorTM 647 (ThermoFisher, I32450) and (in mM): 140 NaCl, 10 HEPES, 2.5 KCl, 1 NaH_2PO_4 , 10 glucose, 2 CaCl_2 , 1 MgCl_2 (pH = 7.4). IB4 binds α -D-galactose groups in the basement membrane of capillaries.¹⁷ Human tissue was fixed for immunohistochemistry in 4% paraformaldehyde for 30 min at room temperature on a shaker.

Cortical slice capillary pericyte imaging

Acute cerebral cortical slices were perfused at a rate of 3–5 ml/min with heated (~34°C) artificial cerebrospinal fluid (aCSF) solution containing (in mM) 124 NaCl, 2.5 KCl, 26 NaHCO_3 , 1 MgCl_2 , 1 NaH_2PO_4 , 10 glucose, 1 ascorbate and 2 CaCl_2 . The aCSF was gassed with 20% O_2 , 5% CO_2 , 75% N_2 . Capillary pericyte imaging was performed in the cortex at 30–100 μm depth. Brightfield imaging was performed using an Olympus BW51 microscope equipped with differential interference contrast (DIC), a 40x water immersion objective, a Coolsnap HQ2 CCD camera, and ImagePro Plus (Media Cybernetics) or Metafluor (Molecular Devices) acquisition softwares. Images were acquired every 5–30 s, with an exposure time of 50 ms. The pixel size was 160 nm. Internal capillary diameters were measured by manually placing a measurement line perpendicular to the capillary at pericyte somata using MetaMorph or ImageJ software. Two-photon imaging was performed using a Zeiss LSM780 microscope with the two-photon laser (Ti:sapphire Mai Tai DeepSee, Spectra Physics) tuned to 940 nm. Cortical pericytes were imaged by acquiring Z-stacks (of size 50–120 \times 50–120 \times 30–40 μm in the x, y and z dimensions respectively, with 2 μm step size, 150 to 300 nm pixel size, and 1.3–2.7 μs pixel dwell time) every 10 s continuously for 10–15 minutes using a 20x/1.0 NA water immersion objective (W Plan-Apochromat, Zeiss). Emitted fluorescence was spectrally divided by a 555-nm dichroic mirror and collected by GaAsP detectors. The power under the objective did not exceed 20 mW. Image processing was performed in FIJI. To account for movements in the x- and y-dimensions, image stacks were projected at maximum intensity in the z-dimension and co-registered using the StackReg plugin in FIJI. Changes in GCaMP5G fluorescence were measured by drawing regions of interest (ROIs) over the soma in FIJI and by normalizing each intensity value to the baseline average.

Noradrenaline (NA; Sigma A7256) oxidation was reduced by supplementing aCSF with 100 μM ascorbic acid and by adding NA powder to the aCSF immediately before imaging. For tetrodotoxin citrate (TTX, Abcam ab120055) experiments, TTX was applied 5 min prior to and in the continuous presence of NA.

For endothelin-1 (ET-1; Sigma E7764) experiments, NA was applied 15 min prior to ET-1. For atipamezole experiments, atipamezole (Sigma; A9611) was applied 15 min prior to NA. Clonidine (Sigma C7897) and xylazine (Rompun, 321350RX) were applied following a 5 min baseline. NA, clonidine and xylazine are photosensitive and were protected from light at all times. Control and drug experiments were interleaved without blinding during experiments and analysis.

In vivo two-photon imaging

Adult NG2-dsRed mice were anesthetised using urethane (1.55 g/kg given in two doses 15 minutes apart; Sigma-Aldrich, #94300) and anesthesia was confirmed by the lack of a withdrawal reflex to a paw pinch. Body temperature was maintained at 36–37°C using a feedback-controlled heating pad. Eyes were protected from drying by applying polyacrylic acid eye drops (Dr. Winzer Pharma GmbH). The trachea was cannulated and mice were mechanically ventilated with medical air supplemented with oxygen using a MiniVent (Model 845). The skull was exposed, slightly thinned using a drill and dried using compressed air. A custom-made headplate was centred over the right barrel cortex, 3 mm laterally from the midline and immediately caudal to the coronal suture. The headplate was attached using superglue gel and mice were head fixed to a custom-built stage. A craniotomy of approximately 2 mm diameter was performed, the dura was removed and HEPES-buffered aCSF was added to the exposed cortex.

Two-photon images of NG2-dsRed labelled pial arteries, penetrating arterioles and capillary pericytes were acquired at a wavelength of 1000 nm. Outer capillary diameters were measured at pericyte somata by drawing lines across vessels perpendicular to their axes in FIJI. The change in diameter upon application of atipamezole (100 μM) to the exposed cortex was measured. The mean laser power in the focal plane did not exceed 34 mW for any experiment.

Immunohistochemistry

Adult NG2-dsRed mice were perfused at 9 ml/min with 20 ml of ice-cold PBS, followed by 20 ml of ice-cold 4% PFA. Brains were extracted and drop-fixed in 4% PFA overnight. Following 3 \times 5 min washes in PBS, sagittal brain slices 100 μm thick were cut in PBS using a Leica VT1200S vibratome. Slices were blocked at 4°C overnight on a shaker, incubated with anti-tyrosine hydroxylase antibody (1:200, raised in chicken, Abcam ab76442) and (in some experiments) anti-dopamine beta hydroxylase antibody (1:200, rabbit, Abcam ab209487) overnight, washed 3 \times 5 min in PBS and incubated with anti-chicken IgG Cy5 (1:500,

Bethyl Labs A30-206C5), anti-chicken IgY Alexa Fluor™ 488 (1:500, Sigma A-11039) and anti-rabbit IgG Alexa Fluor™ 647 (1:500, A31573) for 8 hours. Slices were washed 3×5 min in PBS and cleared overnight at room temperature on a shaker in CUBIC reagent 1 (CUBIC-R1) solution containing 25 wt % urea, 25 wt % *N,N,N',N'*-Tetrakis(2-Hydroxypropyl) ethylenediamine and 15 wt % Triton X-100 (Susaki et al., 2014). Slices were mounted using CUBIC-R1 and image stacks were acquired using a Zeiss LSM 700 confocal microscope using a 20 \times objective. Image stacks were segmented in Imaris and the shortest distance from a TH-labeled process to the closest part of the surface of the nearest pericyte soma, or to the surface of the SMCs at the middle of an arteriole, was measured in 3D using the MeasurementPro module of Imaris. Depending on the size of IB4 labelled human tissue, washing steps in between antibody applications were prolonged, varying from 4–5 washes over 2–8 hours. The incubation period of the anti-TH antibody was 24–72 hours and that of the secondary antibody 24 hrs. Human tissue was cleared at room temperature for up to 9 days (CUBIC-R1 solution was exchanged every 24–48 hours). Tissue was mounted in CUBIC-R1 solution using a custom-made glass chamber and confocal imaged using a 20 \times air objective. The closest distance from the pericyte soma centre to a TH-labelled process was measured in FIJI.

Statistics

Statistical tests were performed in Prism 6 (GraphPad Software Inc., CA, USA). The D'Agostino-Pearson omnibus test was used to assess the normality of data. For non-normally distributed data, a non-parametric statistical analysis was performed using the Mann-Whitney U Test (comparing 2 groups, unpaired) or a Wilcoxon matched-pairs signed rank test (comparing 2 groups, paired). For normally distributed data, a parametric test was used: p-values were determined using a homoscedastic (equal variance) or heteroscedastic (unequal variance, with Welch's correction) two-tailed Student's t-test (comparing 2 groups) or one-way ANOVA with a Tukey *post hoc* test (comparing >2 groups). These procedures include correction for multiple comparisons within each figure panel. Bars show the mean \pm standard deviation. P-values <0.05 were considered significant and all tests were 2-tailed.

Results

Noradrenaline release sites in the cerebral cortex

Immunohistochemistry using an antibody to tyrosine hydroxylase, the rate-limiting enzyme for catecholamine

synthesis which labels noradrenergic and dopaminergic axons including those of locus coeruleus neurons,^{18,19} revealed catecholamine-containing axons ramifying extensively in the cerebral cortex of mice in which pericytes and some vascular smooth muscle cells (SMCs) were labelled transgenically by dsRed expression under control of the NG2 promoter (Figure 1(a)). Consistent with previous data,^{7,9} TH-labeled varicosities were found close to capillary pericytes and to arteriolar SMCs (Figure 1(b)). The mean distance to the nearest varicosity was $\sim 6 \mu\text{m}$ for pericytes (independent of capillary branch order, traced from the penetrating arteriole as in Figure 1(a)) and $\sim 12 \mu\text{m}$ for SMCs (Figure 1(c)). Labeling for dopamine beta hydroxylase (DBH; the enzyme that converts dopamine into noradrenaline, which is hence more specific for noradrenergic axons) revealed a similar distance to pericytes ($\sim 5 \mu\text{m}$) and SMCs ($\sim 18 \mu\text{m}$), suggesting that capillary pericytes receive most of the vascular noradrenergic innervation in the rodent cerebral cortex (Figure 1(d)).

Human cortical tissue obtained from neurosurgical operations exhibited similar tyrosine hydroxylase labelling (Figure 1(e)) with a mean distance of $\sim 12 \mu\text{m}$ from pericytes to the nearest varicosity (Figure 1(f)).

Noradrenaline does not evoke contraction by raising $[\text{Ca}^{2+}]_i$

Imaging capillaries in rat brain cortical slices (Figure 2 (a)) confirmed that application of NA (between 2 and 200 μM) led to capillary constriction near pericyte somata (Figure 2(b) and (c)).^{6,10} If noradrenaline evokes pericyte contraction by acting on G_q -coupled α_1 receptors, then it should raise $[\text{Ca}^{2+}]_i$ by releasing calcium from intracellular stores. However, in cortical slices from mice expressing the Ca^{2+} -sensor GCaMP5G in pericytes (see Materials and Methods), we found that NA evoked no significant rise of $[\text{Ca}^{2+}]_i$ in pericyte somata or processes, even when TTX was present to prevent any changes of neuronal activity induced by NA (Figure 2(d) and (e), Fig. S1A). This was not due to the GCaMP5G sensor being ineffectual because endothelin-1 (ET-1, 10 nM), which acts on G_q PCRs to release Ca^{2+} from internal stores,^{6,20} evoked a robust $[\text{Ca}^{2+}]_i$ rise (Figure 2(d) and (f)). Similarly, NA evoked no detectable rise in $[\text{Ca}^{2+}]_i$ in arteriolar SMCs (Figure 2(g)). Consistent with the pericyte-mediated capillary constriction not being mediated by activation of α_1 receptors and release of Ca^{2+} from internal stores, the α_1 receptor agonist phenylephrine (PE, 1 μM) evoked no significant $[\text{Ca}^{2+}]_i$ rise in pericytes nor a pericyte-mediated constriction of capillaries (Figure 2(h) to (i), Fig. S1B). PE also did not raise $[\text{Ca}^{2+}]_i$ in SMCs of pial arteries and did not constrict them (Fig. S1C-E).

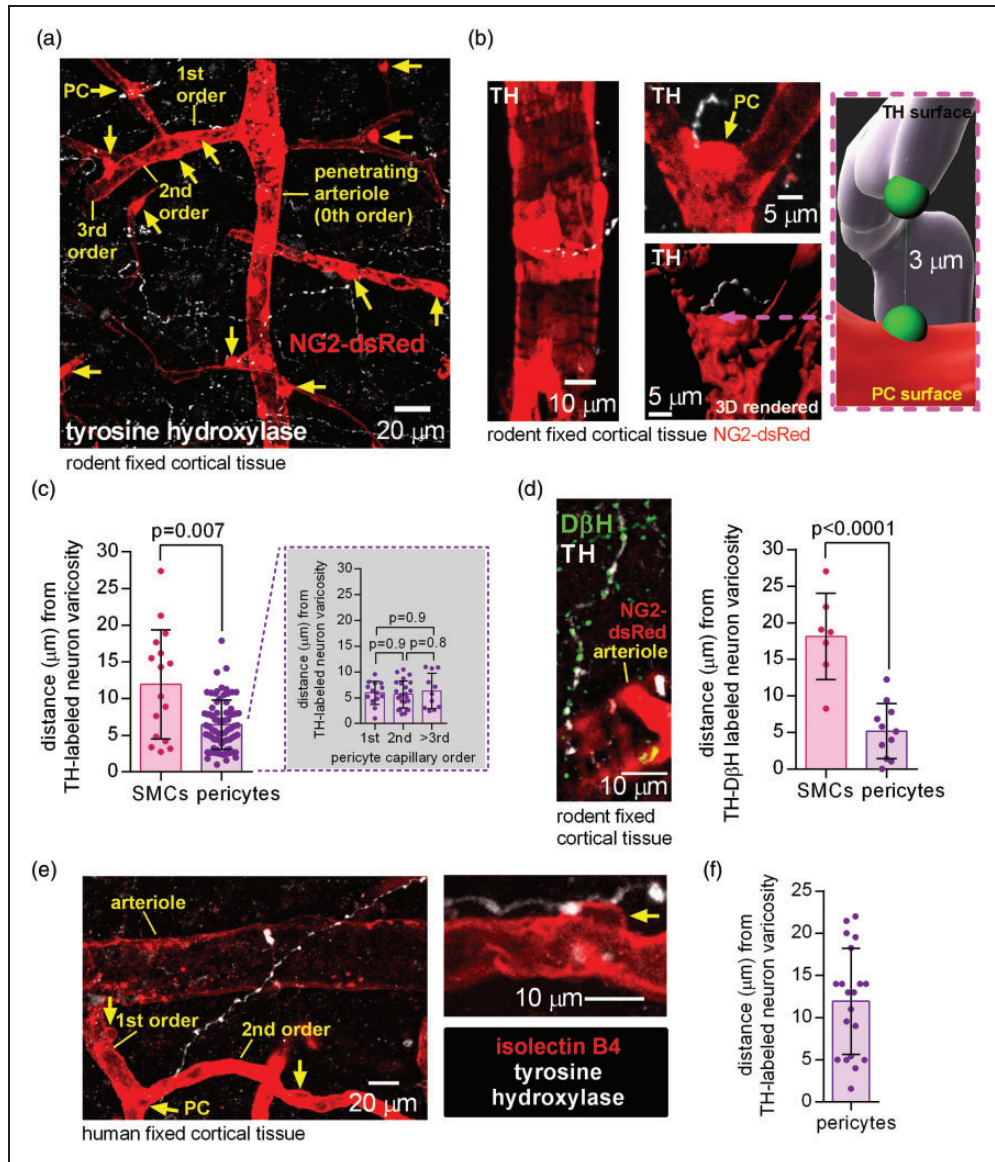


Figure 1. Tyrosine hydroxylase- and D β H-labelled axons are in close proximity to rodent and human pericytes in the cerebral cortex. (a) Maximum intensity projection confocal image of tyrosine hydroxylase (TH) labelled axon varicosities (white, potential LC axon transmitter release sites) and pericytes (PC, yellow arrows) and arteriole smooth muscle cells (SMCs) labelled using dsRed under the NG2 promoter in the cortex of an adult NG2-dsRed mouse. The capillary branching order from the penetrating arteriole (0th order) is indicated. (b) Higher magnification images: left, TH-labelled axon near arteriole; right, two 3D views (rendered in Imaris) of a pericyte (arrow) at a capillary branch point and TH-labelled axon. Inset shows measurement in 3D of the shortest distance from a TH-labeled varicosity surface to the surface of the nearest soma (green blobs are to indicate the end of the measurement line). (c) Nearest TH-labelled varicosities are closer to pericyte somata than to arteriolar smooth muscle cells (chosen to be half way up the penetrating arteriole), independent of capillary branch order ($n = 16$ arterioles and 76 pericytes from 3 mice). (d) Left: Co-labelling for TH and dopamine beta hydroxylase (D β H) to define noradrenergic axons. Right: Varicosities labelled for both TH and D β H are located closer to pericyte somata than to SMCs ($n = 7$ SMCs and 11 pericytes from 3 mice). (e) Confocal image (single plane) of TH-labelled axon and isolectin B4 (IB4) labelled arteriole, capillaries and pericytes (arrows) in human cortical tissue and (f) Nearest TH-labelled axon to pericyte soma distance in human cortical tissue (20 pericytes from 3 humans).

It has previously been suggested¹³ that NA-evoked $[Ca^{2+}]_i$ transients in astrocytes trigger release of the arachidonic acid derivative 20-HETE which evokes contraction of arteriolar SMCs. However, the NA-evoked

capillary constriction in brain slices was unaffected by blocking 20-HETE synthesis with 100 nM HET0016 (Figure 2(j), not significantly different, $p = 0.4$), as found previously for cerebellar pericytes.⁵

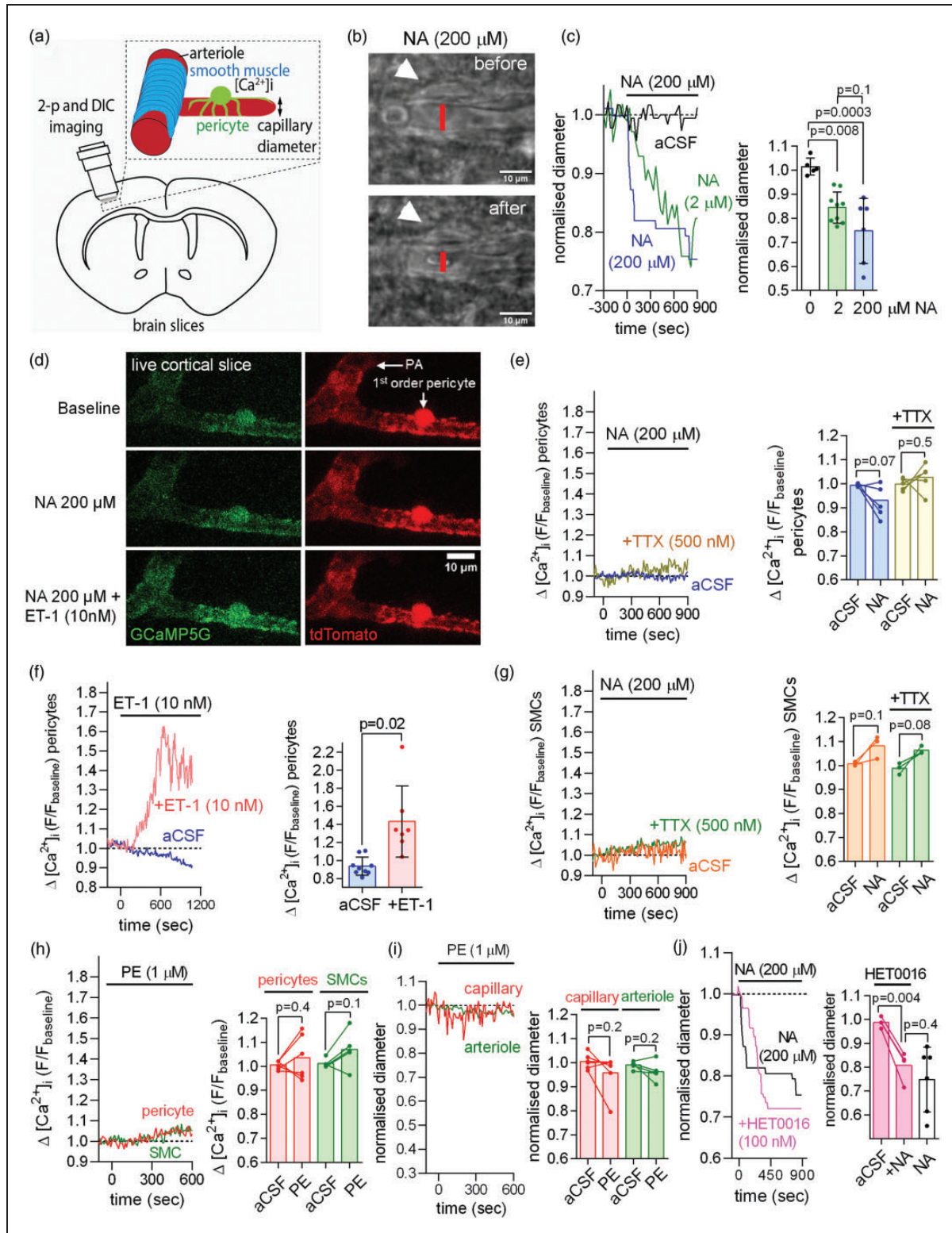


Figure 2. Noradrenaline (NA) contracts capillary pericytes without raising pericyte $[\text{Ca}^{2+}]_i$ in acute rodent cerebral cortical slices. (a) Capillary diameter or somatic $[\text{Ca}^{2+}]_i$ was measured in acute cortical slices using two-photon (2-p) or differential interference contrast (DIC) imaging to capture the onset of the NA-evoked contraction (DIC images acquired every 5–30 sec and 2-p stacks every 10 sec). (b) DIC image of rat cortical capillary with pericyte (white arrow) before and after stimulation with 200 μM noradrenaline (NA). The lumen diameter was measured at the pericyte soma as indicated by the red line. (c) Left: Exemplar time course of

Continued.

Noradrenaline evokes contraction by activating α_2 receptors

The α_2 receptor blocker atipamezole (1 μM) did not affect capillary diameter when applied alone in brain slices (Figure 3(a), presumably because there is little NA release in slices where the locus coeruleus axons are cut), but completely blocked the NA-evoked capillary constriction (Figure 3(b)). Conversely, the α_2 agonists clonidine (20 μM) and xylazine (50 μM) both evoked a capillary constriction near pericytes of a magnitude similar to that evoked by NA (Figure 3(c)).

When imaging capillaries, penetrating arterioles and pial arteries through a cranial window *in vivo* (Figure 3(d)), application of atipamezole to the surface of the cortex resulted in a dilation of capillaries near pericyte somata (Figure 3(e)), indicating that there is tonic activation *in vivo* of the contractile mechanism characterised here, presumably by NA released from locus coeruleus axons. The penetrating arterioles and pial arteries similarly dilated (Figure 3(e)).

These data suggest that, for both parenchymal capillaries and arteriolar/arterial SMCs, NA evokes contraction by a mechanism other than activation of α_1 receptors. Although we cannot be sure that NA acts directly on pericytes (or SMCs), for simplicity we propose that NA released from LC axons acts on α_2 receptors to lower the cAMP level in pericytes, leading to a fall of myosin light chain phosphatase activity and a resulting increase in contractile tone (Figure 3(f)).²¹

Discussion

Noradrenaline, which can act via volume transmission at some distance from its release site, is known to affect neuronal information processing via its direct actions on neurons, for example by modulating neurotransmitter release at synaptic terminals²² and by depolarizing neurons (via inhibition of their K^+ conductance and activation of hyperpolarization-activated I_h channels).²³ However, NA also regulates cerebral blood

flow by evoking contractile tone of arterioles and capillary pericytes, which may have indirect effects on neuronal function. The relative importance of these effects in NA-mediated changes in attention and arousal are rarely discussed, although the volume transmission aspect of NA-evoked effects must mean that they cannot be controlled separately.

It is commonly assumed that effects of NA on blood flow are mediated by activation of Ca^{2+} -mobilising α_1 receptors on contractile cells.¹¹ Here we have investigated how NA affects the contractile tone of capillary pericytes, because capillaries comprise the majority of the resistance to cerebral blood flow within the brain parenchyma.^{2,3} Surprisingly, we found that although superfused NA made pericytes contract, and constrict capillaries, it did not raise pericyte $[\text{Ca}^{2+}]_i$ (Figure 2(a) to (f)). Furthermore the α_1 receptor agonist phenylephrine did not raise pericyte $[\text{Ca}^{2+}]_i$ or evoke contraction (Figure 2(h) to (i)). In contrast, the NA-evoked contraction was abolished by the α_2 receptor antagonist atipamezole (Figure 3(b)), and mimicked by α_2 receptor agonists (Figure 3(c)), implying that NA evokes contraction by an unexpected mechanism dependent on α_2 receptors (Figure 3(f)).

We presume these α_2 receptors to be on pericytes themselves (rather than on some other cell type that releases a messenger to raise pericyte $[\text{Ca}^{2+}]_i$) because NA evoked pericyte contraction without raising pericyte $[\text{Ca}^{2+}]_i$. Since α_2 receptors are G_i -coupled, their activation by NA will lower the pericyte cyclic AMP concentration, which we assume promotes contraction by leading to a decrease of myosin light chain phosphatase activity (Figure 3(f)).²⁴ These data are consistent with radioligand binding studies reporting the presence of α_2 and lack of α_1 receptors on cerebral pericytes.²⁵ Thus, although it is impossible to rule out the possibility that the preparation of brain slices somehow inactivates pericyte α_1 receptors, the most parsimonious interpretation of our data is that NA evokes pericyte contraction by acting on α_2 receptors. Furthermore,

Figure 2. Continued.

NA-evoked capillary constriction measured at the pericyte soma in response to aCSF containing 0, 2 or 200 μM NA. Right: Mean capillary constriction after 15 mins ($n = 5$ in aCSF from 3 rats; $n = 9$ for 2 μM NA from 9 rats; $n = 6$ for 200 μM NA from 3 rats). (d) Two-photon images of penetrating arteriole (PA) smooth muscle cells (SMCs) and 1st order capillary pericyte expressing GCaMP5g and tdTomato in NG2-Cre^{ERT2}-GCaMP5g mice. (e) Left: time course of mouse pericyte $[\text{Ca}^{2+}]_i$ in response to NA in the presence or absence of TTX. Right: NA does not raise pericyte $[\text{Ca}^{2+}]_i$ in the presence or absence of TTX ($n = 6$ pericytes for NA from 3 mice; $n = 5$ pericytes for NA+TTX from 3 mice). (f) After 10 min of pre-incubation with NA (not shown), application of the Gq-coupled agonist endothelin-1 (ET-1) in the continuous presence of NA raises mouse pericyte $[\text{Ca}^{2+}]_i$ as compared to continuous NA application alone (slow decline of fluorescence may reflect bleaching; $n = 9$ pericytes for NA from 3 mice; $n = 7$ for NA+ET-1 from 3 mice). (g) NA does not raise mouse arteriolar smooth muscle cell (SMC) $[\text{Ca}^{2+}]_i$ in the presence or absence of TTX ($n = 3$ for NA from 3 mice; $n = 3$ for NA+ET-1 from 3 mice). (h–i) The α_1 agonist phenylephrine (1 μM) does not raise $[\text{Ca}^{2+}]_i$ (h) in mouse cortical pericytes ($n = 6$ from 3 mice) or arteriolar SMCs ($n = 5$ from 3 mice) nor decrease capillary or arteriole diameter (i). (j) The 20-HETE synthesis inhibitor HET0016 (100 nM) had no significant effect on the NA-evoked capillary constriction at pericytes ($n = 4$ from 3 rats, data without HET0016 are replotted from panel c).

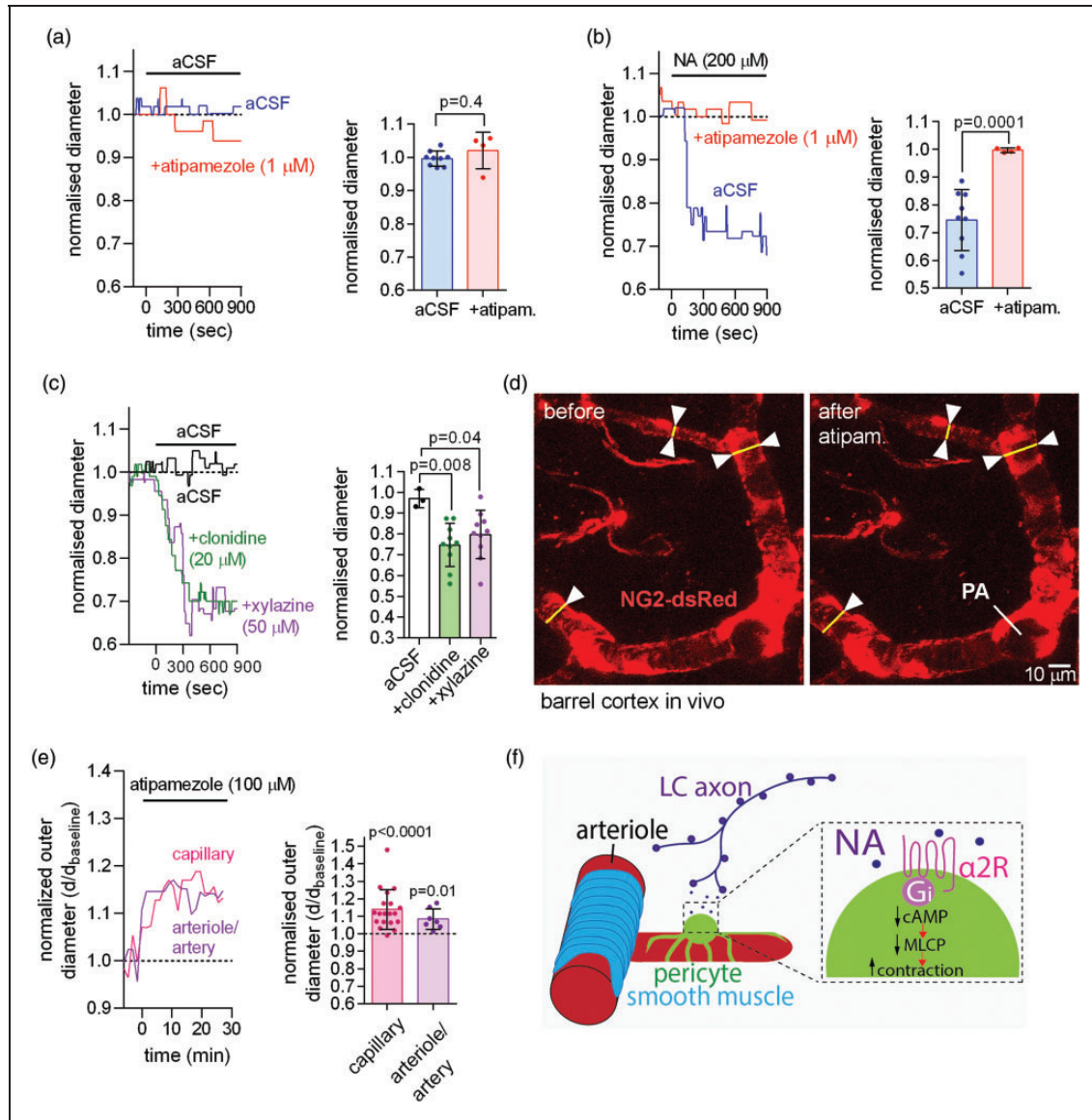


Figure 3. NA contracts capillary pericytes via activation of α_2 adrenergic receptors. (a) Left: time course of normalised capillary diameter at the pericyte soma in the absence or presence of the α_2 receptor blocker atipamezole in acute cortical slices of P21 rats. Right: blocking α_2 receptors with atipamezole had no effect on capillary diameter ($n = 9$ pericytes for aCSF from 6 rats; $n = 4$ for atipamezole from 3 rats). (b) Blocking α_2 receptors with atipamezole greatly reduced the NA-evoked capillary constriction ($n = 9$ for NA from 6 rats; $n = 4$ for NA + atipamezole from 3 rats). (c) Stimulating α_2 receptors with xylazine or clonidine induced a capillary constriction similar to that evoked by application of NA (aCSF 3 pericytes from 3 rats; clonidine 10 pericytes from 4 rats; xylazine 10 pericytes from 3 rats). (d) Imaging of somatosensory cortex through a cranial window in NG2-dsRed mice with penetrating arteriole (PA) and capillary pericytes indicated. (e) *In vivo* application of atipamezole (100 μ M) to the cortical surface evoked a tonic dilation of capillaries at pericytes ($n = 19$ from 3 mice), and of penetrating arterioles and pial arteries ($n = 7$ from 3 mice) and (f) Proposed mechanism by which NA released from LC axons confers contractile tone via G_i protein-coupled α_2 receptors, which lower [cAMP], thus reducing the dephosphorylation of myosin by myosin light chain phosphatase (MLCP).

consistent with this, direct application of the α_2 blocker atipamezole to the cortex *in vivo* evoked dilation of capillaries and arterioles/arteries (Figure 3(d) to (e)).

While published RNA sequencing datasets indicate low α_1 and α_2 receptor expression in pericytes,^{26,27} RNA sequencing is limiting in its detection of weakly

expressed transcripts such as plasma membrane receptors and it is increasingly reported that there can be little correlation between transcript and protein levels.^{28–30} The use of improved dissociation protocols for RNA sequencing,³¹ spatial transcriptomic approaches (that use intact tissue sections) and

development of specific antibodies against adrenergic receptors may be required to further assess the adrenergic receptor expression profile in pericytes. Moreover *in vivo* studies, for example locally puffing NA onto pericytes or optogenetically stimulating or suppressing the release of NA from LC axons,^{32,33} using image acquisition speeds sufficient to capture fast $[Ca^{2+}]_i$ transients³⁴ may help to further assess the effect of NA on contractile tone *in vivo*.

LC stimulation has generally been shown to decrease CBF^{35–40} (with one exception⁴¹ reporting an increase in CBF) whereas LC lesioning increases⁴² or evokes no change^{43,44} in CBF possibly depending on the species, age or brain area studied. In our experiments, direct application of atipamezole to the cortex *in vivo* evoked dilation of capillaries and arterioles/arteries (Figure 3(d) and (e)). This contrasts with the vascular effects evoked by systemic atipamezole administration, which is expected to also block α_2 receptors on neuronal cell bodies in the LC - this blocks α_2 receptor mediated feedback inhibition of NA release by LC neurons, raises cortical NA levels and thus evokes vasoconstriction (at least at the arteriole level).^{45,46}

Although the relative importance of contractile pericytes and arteriolar smooth muscle cells in controlling CBF has been debated, a large fraction of the intraparenchymal resistance of the cerebral vasculature lies in capillaries,^{2,3} and it is now known that even mid-capillary bed pericytes are contractile and can regulate blood flow.^{47,48} The constriction of capillaries by NA provides essential tone so that, when neurons are active and they and their associated astrocytes release vasodilators, an increase of capillary diameter is possible. The degree of dilation possible may depend importantly on the noradrenergic tone being generated, with a greater dilation and fractional increase of blood flow being possible when there is more initial constriction.⁴⁹ This phenomenon may complicate the interpretation of changes of BOLD fMRI signals in conditions when noradrenergic tone is altered, e.g. in states of altered arousal. For instance, NA release from LC axons is decreased during sleep,^{50–52} which may contribute to CBF increases by up to 80% during rapid eye movement (REM) sleep⁵³ when extracellular brain NA levels are lowest.^{51,52} While an increase in arterial CO₂ tension (PaCO₂) induced by respiratory changes also likely contributes to increases in CBF during REM sleep, this increase in CBF is greater than would be predicted from changes in PaCO₂.⁵⁴ Importantly a recent study suggests that the amplitude of cortical NA oscillations may shape transition states between wakefulness and REM and non-REM sleep,³³ raising the possibility that NA drives fluctuations in CBF depending on the arousal state of the brain.⁵⁵

Furthermore, these data imply that blood-brain barrier permeable agents acting on α_2 receptors will alter CBF. In a medical and veterinary setting such agents include the sedative and anaesthetic xylazine, clonidine (which is used to treat dysmenorrhea, hypertension, Tourette's, menopausal symptoms and alcohol/opiate withdrawal) and methyldopa (used to treat hypertension, including in pregnancy).

Funding

The author(s) disclosed receipt of the following financial support for the research, authorship, and/or publication of this article: The study was supported by a BBSRC LiDO PhD studentship to NK, an MRC CARP award to GJ, an HRH Princess Chulabhorn College of Medical Science scholarship to CH, and an ERC Advanced Investigator Award (740427, BrainEnergy) and Wellcome Trust Senior Investigator Award (099222/Z/12/Z) to DA. The funders played no role in any part of the study.

Declaration of conflicting interests

The author(s) declared no potential conflicts of interest with respect to the research, authorship, and/or publication of this article.

Authors' contributions

Nils Korte: Concept and design, acquisition of data, analysis and interpretation of data, review and editing.

Greg James, Haoming You: Acquisition of data, analysis and interpretation of data, review and editing.

Chanawee Hirunpattarasilp, Isabel Christie: Acquisition of data, supervision, review and editing.

Huma Sethi: Provision of human tissue, review and editing.

David Attwell: Concept and design, interpretation of data, writing manuscript, supervision.

Code availability

Not applicable

Ethics approval and consent to participate


Ethical approval from the National Health Service (REC number 12/NW/0568) and informed consent from all patients were obtained.

Availability of data and material

Datasets are available from the corresponding author.

ORCID iDs

Isabel Christie  <https://orcid.org/0000-0003-0982-0331>

David Attwell  <https://orcid.org/0000-0003-3618-0843>

Supplementary material

Supplemental material for this article is available online.

References

1. Attwell D, Buchan AM, Charkpak S, et al. Glial and neuronal control of brain blood flow. *Nature* 2010; 468: 232–243.
2. Blinder P, Tsai PS, Kaufhold JP, et al. The cortical angiome: an interconnected vascular network with non-columnar patterns of blood flow. *Nat Neurosci* 2013; 16: 889–897.
3. Gould IG, Tsai P, Kleinfeld D, et al. The capillary bed offers the largest hemodynamic resistance to the cortical blood supply. *J Cereb Blood Flow Metab* 2017; 37: 52–68.
4. Mishra A, Reynolds JP, Chen Y, et al. Astrocytes mediate neurovascular signaling to capillary pericytes but not to arterioles. *Nat Neurosci* 2016; 19: 1619–1627.
5. Hall CN, Reynell C, Gesslein B, et al. Capillary pericytes regulate cerebral blood flow in health and disease. *Nature* 2014; 508: 55–60.
6. Nortley R, Korte N, Izquierdo P, et al. Amyloid β oligomers constrict human capillaries in Alzheimer's disease via signaling to pericytes. *Science* 2019; 365: eaav9518.
7. Giorgi FS, Galgani A, Puglisi-Allegra S, et al. Locus coeruleus and neurovascular unit: from its role in physiology to its potential role in Alzheimer's disease. *J Neurosci Res* 2020; 98: 2406–2434.
8. Robertson SD, Plummer NW, de Marchena J, et al. Developmental origins of central norepinephrine neuron diversity. *Nat Neurosci* 2013; 16: 1016–1023.
9. Cohen Z, Molinatti G and Hamel E. Astroglial and vascular interactions of noradrenaline terminals in the rat cerebral cortex. *J Cereb Blood Flow Metab* 1997; 17: 894–904.
10. Peppiatt CM, Howarth C, Mobbs P, et al. Bidirectional control of CNS capillary diameter by pericytes. *Nature* 2006; 443: 700–704.
11. Motiejunaite J, Amar L and Vidal-Petiot E. Adrenergic receptors and cardiovascular effects of catecholamines. *Ann Endocrinol (Paris)* 2021; 82: 193–197.
12. Duffy S and MacVicar BA. Adrenergic calcium signaling in astrocyte networks within the hippocampal slice. *J Neurosci* 1995; 15: 5535–5550.
13. Mulligan SJ and MacVicar BA. Calcium transients in astrocyte endfeet cause cerebrovascular constrictions. *Nature* 2004; 431: 195–199.
14. Zhu X, Bergles DE and Nishiyama A. NG2 cells generate both oligodendrocytes and grey matter astrocytes. *Development* 2008; 135: 145–157.
15. Huang W, Zhao N, Bai X, et al. Novel NG2-CreERT2 knock-in mice demonstrate heterogeneous differentiation potential of NG2 glia during development. *Glia* 2014; 62: 896–913.
16. Gee JM, Smith NA, Fernandez FR, et al. Imaging activity in neurons and glia with a Polr2a-based and cre-dependent GCaMP5G-IRES-tdTomato reporter mouse. *Neuron* 2014; 83: 1058–1072.
17. Peters BP and Goldstein IJ. The use of fluorescein-conjugated *Bandeiraea simplicifolia* B4-isolectin as a histochemical reagent for the detection of alpha-D-galactopyranosyl groups. Their occurrence in basement membranes. *Exp Cell Res* 1979; 120: 321–334.
18. Pickel VM, Joh TH and Reis DJ. Ultrastructural localization of tyrosine hydroxylase in noradrenergic neurons of brain. *Proc Natl Acad Sci U S A* 1975; 72: 659–663.
19. Schmidt K, Bari B, Ralle M, et al. Localization of the locus coeruleus in the mouse brain. *J Vis Exp* 2019; 145: DOI:10.3791/58652.
20. Korte N, Ilkan Z, Pearson CL, et al. The Ca²⁺-gated channel TMEM16A amplifies capillary pericyte contraction and reduces cerebral blood flow after ischemia. *J Clin Invest* 2022; 132: e154118.
21. Ito M, Okamoto R, Ito H, et al. Regulation of myosin light-chain phosphorylation and its roles in cardiovascular physiology and pathophysiology. *Hypertens Res* 2022; 45: 40–52.
22. Bertolino M, Vicini S, Gillis R, et al. Presynaptic alpha2-adrenoceptors inhibit excitatory synaptic transmission in rat brain stem. *Am J Physiol* 1997; 272: G654–G661.
23. Bergles DE, Doze VA, Madison DV, et al. Excitatory actions of norepinephrine on multiple classes of hippocampal interneurons. *J Neurosci* 1996; 16: 572–585.
24. Azam MA, Yoshioka K, Ohkura S, et al. Ca²⁺-independent, inhibitory effects of cyclic adenosine 5'-monophosphate on Ca²⁺ regulation of phosphoinositide 3-kinase, C2alpha, rho, and myosin phosphatase in vascular smooth muscle. *J Pharmacol Exp Ther* 2007; 320: 907–916.
25. Elfont RM, Sundaresan PR and Sladek CD. Adrenergic receptors on cerebral microvessels: pericyte contribution. *Am J Physiol* 1989; 256: R224–R230.
26. L, Manno G, Siletti K, Furlan A, et al. Molecular architecture of the developing mouse brain. *Nature* 2021; 596: 92–96.
27. Vanlandewijck M, He L, Mäe MA, et al. A molecular atlas of cell types and zonation in the brain vasculature [published correction appears in nature. *Nature* 2018; 554: 475–480.
28. Liu Y, Beyer A and Aebersold R. On the dependency of cellular protein levels on mRNA abundance. *Cell* 2016; 165: 535–550.
29. Johnson ECB, Carter EK, Dammer EB, et al. Large-scale deep multi-layer analysis of Alzheimer's disease brain reveals strong proteomic disease-related changes not observed at the RNA level. *Nat Neurosci* 2022; 25: 213–225.
30. Caldwell ALM, Sancho L, Deng J, et al. Aberrant astrocyte protein secretion contributes to altered neuronal development in multiple models of neurodevelopmental disorders. *Nat Neurosci* 2022; 25: 1163–1178.
31. Marsh SE, Walker AJ, Kamath T, et al. Dissection of artifactual and confounding glial signatures by single-cell sequencing of mouse and human brain. *Nat Neurosci* 2022; 25: 306–316.
32. Oe Y, Wang X, Patriarchi T, et al. Distinct temporal integration of noradrenaline signaling by astrocytic second messengers during vigilance. *Nat Commun* 2020; 11: 471.

33. Kjaerby C, Andersen M, Hauglund N, et al. Memory-enhancing properties of sleep depend on the oscillatory amplitude of norepinephrine. *Nat Neurosci* 2022; 25: 1059–1070.
34. Gonzales AL, Klug NR, Moshkforoush A, et al. Contractile pericytes determine the direction of blood flow at capillary junctions. *Proc Natl Acad Sci U S A* 2020; 117: 27022–27033.
35. Buchweitz E, Edelman NH and Weiss HR. Effect of locus coeruleus stimulation on regional cerebral oxygen consumption in the cat. *Brain Res* 1985; 325: 107–114.
36. de la Torre JC, Surgeon JW and Walker RH. Effects of locus coeruleus stimulation on cerebral blood flow in selected brain regions. *Acta Neurol Scand Suppl* 1977; 64: 104–105.
37. Goadsby PJ and Duckworth JW. Low frequency stimulation of the locus coeruleus reduces regional cerebral blood flow in the spinalized cat. *Brain Res* 1989; 476: 71–77.
38. Katayama Y, Ueno Y, Tsukiyama T, et al. Long lasting suppression of firing of cortical neurons and decrease in cortical blood flow following train pulse stimulation of the locus coeruleus in the cat. *Brain Res* 1981; 216: 173–179.
39. Ohta K, Gotoh F, Shimazu K, et al. Locus coeruleus stimulation exerts different influences on the dynamic changes of cerebral pial and intraparenchymal vessels. *Neurol Res* 1991; 13: 164–167.
40. Raichle ME, Hartman BK, Eichling JO, et al. Central noradrenergic regulation of cerebral blood flow and vascular permeability. *Proc Natl Acad Sci U S A* 1975; 72: 3726–3730.
41. Toussay X, Basu K, Lacoste B, et al. Locus coeruleus stimulation recruits a broad cortical neuronal network and increases cortical perfusion. *J Neurosci* 2013; 33: 3390–3401.
42. Bates D, Weinshilboum RM, Campbell RJ, et al. The effect of lesions in the locus coeruleus on the physiological responses of the cerebral blood vessels in cats. *Brain Res* 1977; 136: 431–443.
43. Dahlgren N, Lindvall O, Sakabe T, et al. Cerebral blood flow and oxygen consumption in the rat brain after lesions of the noradrenergic locus coeruleus system. *Brain Res* 1981; 209: 11–23.
44. Reddy SV, Yaksh TL, Anderson RE, et al. Effect in cat of locus coeruleus lesions on the response of cerebral blood flow and cardiac output to altered paco₂. *Brain Res* 1986; 365: 278–288.
45. Bekar LK, Wei HS and Nedergaard M. The locus coeruleus-norepinephrine network optimizes coupling of cerebral blood volume with oxygen demand. *J Cereb Blood Flow Metab* 2012; 32: 2135–2145.
46. Dennis T, L’Heureux R, Carter C, et al. Presynaptic alpha-2 adrenoceptors play a major role in the effects of idazoxan on cortical noradrenaline release (as measured by in vivo dialysis) in the rat. *J Pharmacol Exp Ther* 1987; 241: 642–649.
47. Rungta RL, Chaigneau E, Osmanski BF, et al. Vascular compartmentalization of functional hyperemia from the synapse to the pia. *Neuron* 2018; 99: 362–375.e4.
48. Hartmann DA, Berthiaume AA, Grant RI, et al. Brain capillary pericytes exert a substantial but slow influence on blood flow. *Nat Neurosci* 2021; 24: 633–645.
49. Blanco VM, Javier JE and Filosa JA. Tone-dependent vascular responses to astrocyte-derived signals. *Am J Physiol Heart Circ Physiol* 2008; 294: H2855–2863.
50. Aston-Jones G and Bloom FE. Activity of norepinephrine-containing locus coeruleus neurons in behaving rats anticipates fluctuations in the sleep-waking cycle. *J Neurosci* 1981; 1: 876–886.
51. Léna I, Parrot S, Deschaux O, et al. Variations in extracellular levels of dopamine, noradrenaline, glutamate, and aspartate across the sleep-wake cycle in the medial prefrontal cortex and nucleus accumbens of freely moving rats. *J Neurosci Res* 2005; 81: 891–899.
52. Shouse MN, Staba RJ, Saquib SF, et al. Monoamines and sleep: microdialysis findings in pons and amygdala. *Brain Res* 2000; 860: 181–189.
53. Revich M, Isaacs G, Evarts E, et al. The effect of slow wave sleep and REM sleep on regional cerebral blood flow in cats. *J Neurochem* 1968; 15: 301–306.
54. Santiago TV, Guerra E, Neubauer JA, et al. Correlation between ventilation and brain blood flow during sleep. *J Clin Invest* 1984; 73: 497–506.
55. Turner KL, Gheres KW, Proctor EA, et al. Neurovascular coupling and bilateral connectivity during NREM and REM sleep. *Neuroscience* 2020; 9: e62071.